Neurobiology of Disease 121 (2019) 315–326

Contents lists available at ScienceDirect

Neurobiology of Disease

journal homepage: www.elsevier.com/locate/ynbdi

Role of intracellular Ca^{2+} stores for an impairment of visual processing in a mouse model of Alzheimer's disease

Nithi Asavapanumas[a], Bianca Brawek[a], Peter Martus[b], Olga Garaschuk[a,*]

[a] Institute of Physiology, Department of Neurophysiology, Eberhard Karls University of Tübingen, Tübingen, Germany
[b] Institute for Clinical Epidemiology and Applied Biostatistics, Eberhard Karls University of Tübingen, Tübingen, Germany

ARTICLE INFO

Keywords:
Alzheimer's disease
Neuronal hyperactivity
Calcium stores
Impairment of visual signal processing

ABSTRACT

Besides deficits in memory and cognition, impaired visual processing is common for Alzheimer's disease (AD) patients and mouse models of AD but underlying mechanisms still remain unclear. Using in vivo Ca^{2+} imaging of the mouse primary visual cortex (V1) we tested whether such impairment is caused by neuronal hyperactivity, an emerging functional hallmark of AD. Profound neuronal hyperactivity was indeed found in V1 of APP_{SWE}/$PS1_{G384A}$ and even of $PS1_{G384A}$ mice, presenting neither with plaque accumulation nor with neuroinflammation. This hyperactivity was accompanied by over-responsiveness to visual stimuli and impaired visual tuning properties of individual neurons, largely caused by insufficient suppression of responses to non-preferred orientation/direction stimuli. Moreover, visual stimulation robustly suppressed the ongoing spontaneous activity in WT but not in APP_{SWE}/$PS1_{G384A}$ mice. Emptying intracellular Ca^{2+} stores significantly reduced neuronal hyperactivity and the pathological over-responsiveness to visual stimuli, but could not rescue stimulus-induced suppression of spontaneous activity and impaired tuning properties of individual cells. Thus, our data identify the AD-mediated dysfunction of intracellular Ca^{2+} stores as a main cause of pathologically increased visual responsiveness in APP_{SWE}/$PS1_{G384A}$ mice. At the same time, the impairment of visual tuning and the stimulus-induced suppression of spontaneous activity, identified in this study, are likely caused by different mechanisms as, for example, dysfunction of local interneurons.

1. Introduction

Alzheimer's disease (AD) is a progressive neurodegenerative disorder and a common cause of cognitive impairment in the elderly. The pathological hallmarks of AD include the deposition of misfolded or aggregating proteins in amyloid beta (Aβ) plaques and neurofibrillary tangles, neuroinflammation as well as neuronal Ca^{2+} dyshomeostasis in extreme case leading to neuronal death. Most of AD cases are sporadic, with advancing age being the most critical risk factor. Mutations in amyloid precursor protein (APP), presenilin 1 (PS1) and 2 (PS2) genes are the most common causes of the familial form of AD (Hardy, 1997; Shen and Kelleher III, 2007; Steiner and Haass, 2000; Tandon and Fraser, 2002), representing some 5–10% of all AD cases. Out of all known mutations leading to the familiar form of AD, the majority (> 100 mutations in total) are located on PS1 (Mattson, 2010). On the one hand side, presenilins are important for APP cleavage and represent an integral part of the γ-secretase complex. On the other, they are known to control intracellular Ca^{2+} homeostasis and neurotransmitter release (Bezprozvanny and Mattson, 2008; Chakroborty and Stutzmann, 2014; Hermes et al., 2010; Zhang et al., 2009).

In the recent years, neuronal hyperactivity was recognized as a key functional hallmark of AD. Indeed, neuronal hyperactivity, including subclinical epileptiform activity (spikes and sharp waves) as well as clinically apparent seizures, has been repeatedly reported in both AD patients (Haberman et al., 2017; Palop et al., 2006; Palop and Mucke, 2016) and AD animal models (Busche et al., 2008; Lerdkrai and Garaschuk, 2018; Minkeviciene et al., 2009; Palop et al., 2007; Palop and Mucke, 2016; Siskova et al., 2014). Interestingly, the patients with

Abbreviations: AD, Alzheimer's disease; V1, primary visual cortex; Aβ, amyloid beta; PS1, presenilin 1; PS2, presenilin 2; aMCI, amnestic mild cognitive impairment; VEPs, visually evoked potentials; CPA, cyclopiazonic acid; AD mice, APP_{swe}/$PS1_{G384A}$ mice; PS45 mice, $PS1_{G384A}$ mice; WT mice, wild-type control mice; ROIs, regions of interest; ΔF/F, relative changes in fluorescence; SD, standard deviation; ANOVA, analysis of variance; DSI, direction selectivity index; OSI, orientation selectivity index; rANOVA, repeated measures analysis of variance; LSD, least significant difference; GEE, Generalized estimating equation; AUC, area under the curve; PV^+, parvalbumin-positive neurons

* Corresponding author at: Department of Neurophysiology, University of Tübingen, Keplerstr. 15, 72074 Tübingen, Germany.
E-mail addresses: nithi.asavapanumas@uni-tuebingen.de (N. Asavapanumas), bianca.brawek@uni-tuebingen.de (B. Brawek), Peter.Martus@med.uni-tuebingen.de (P. Martus), olga.garaschuk@uni-tuebingen.de (O. Garaschuk).

https://doi.org/10.1016/j.nbd.2018.10.015
Received 24 July 2018; Received in revised form 28 September 2018; Accepted 22 October 2018
Available online 24 October 2018
0969-9961/

both sporadic and familial forms of AD have a higher propensity for developing seizures (Palop and Mucke, 2016). In addition, patients with amnestic mild cognitive impairment (aMCI) exhibit an increased neuronal activity when compared with age-matched control subjects, and the degree of neuronal hyperactivity correlates with the degree of cognitive impairment (Haberman et al., 2017). Moreover, the cognitive impairment in aMCI patients was significantly improved by reducing neuronal hyperactivity with an antiepileptic drug levetiracetam (Bakker et al., 2012).

Besides the impairment of cognition, AD patients also present with an impairment of sensory processing in different sensory systems (Albers et al., 2015) including olfaction (Daulatzai, 2015; Mesholam et al., 1998) as well as auditory (Gates et al., 2008) and visual processing. Specifically, AD patients show a decrease in contrast sensitivity in all spatial frequency ranges of visual stimuli (Albers et al., 2015; Cronin-Golomb et al., 1991) and are also less capable to detect the direction of visual motion, compared with age-matched controls (Rizzo et al., 2000). Furthermore, visually evoked potentials (VEPs) in AD patients showed a significant reduction of P1 and N1 amplitudes, whereas aMCI patients showed only a reduction of N1 amplitude (Stothart et al., 2015). In addition, the degree of impairment of contrast selectivity and the abnormal VEP in both AD and aMCI patients correlated with the degree of their cognitive impairment (Risacher et al., 2013; Rizzo et al., 2000; Stothart et al., 2015).

In line with patient data described above, in vivo imaging of layer 2/3 neurons in the primary visual cortex (V1) of a mouse model of AD ($APP_{SWE}/PS1_{G384A}$ mice) revealed a significant impairment of visual signal processing. Specifically, neurons of mutant mice showed an impairment of orientation and direction tuning properties (Grienberger et al., 2012). Interestingly, this impairment was seen in hyperactive neurons only, underscoring the relationship between the impairment of visual processing and neuronal hyperactivity. Our recent in vivo study in the frontal/motor cortex of $APP_{SWE}/PS1_{G384A}$ and $PS1_{G384A}$ mice (Lerdkrai et al., 2018) tested the role of the intracellular Ca^{2+} stores for neuronal hyperactivity. In the somato-dendritic compartment of layer 2/3 neurons we found a slight overfilling of the intracellular Ca^{2+} stores of endoplasmic reticulum exclusively in hyperactive cells, and this overfilling was much smaller than what can be inferred from the in vitro data (Goussakov et al., 2010). At the same time the data revealed an important role of intracellular Ca^{2+} stores for controlling amplitude and frequency of axonal Ca^{2+} transients in presynaptic boutons targeting layer 2/3 neurons. Moreover, emptying the intracellular Ca^{2+} stores with cyclopiazonic acid (CPA) as well as blocking the ryanodine receptors with dantrolene caused a significant reduction of neuronal hyperactivity, suggesting that reducing store-mediated neuronal hyperactivity might counteract the impairment of visual processing in mouse models of AD.

In the present study, we employed in vivo two-photon Ca^{2+} imaging of layer 2/3 neurons in V1 to characterize in detail the alterations of visual processing in $APP_{SWE}/PS1_{G384A}$ as well as $PS1_{G384A}$ mice and to understand the relationship between the impairment of visual processing and neuronal hyperactivity. Further, using the newly developed treatment protocol for blocking neuronal hyperactivity (Lerdkrai et al., 2018), we tested whether this treatment is able to ameliorate the deficits in visual processing.

2. Materials and methods

2.1.1. Mice

Experiments were done in 10–12 months old $APP_{swe}/PS1_{G384A}$ mice (AD mice) and heterozygous $PS1_{G384A}$ mice (PS45 mice) of either sex raised on a C57Bl/6 background. In these mouse strains all mutated genes are expressed selectively in neurons under control of the Thy-1 promoter. At the age studied, the AD mice develop robust amyloidosis covering the entire forebrain, so that virtually all neurons are located in plaque vicinity (Lerdkrai et al., 2018). Age-matched C57Bl/6 mice were used as wild-type controls (WT mice). Female animals were maintained in a group (3–5 mice). Male animals were maintained individually. Animals were kept under a 12 h light/dark cycle and were fed ad libitum.

2.1.2. Acute craniotomy and in vivo labeling of neurons

The surgery was conducted as described previously (Garaschuk et al., 2006; Stosiek et al., 2003). Briefly, animals were anesthetized using isoflurane (2.5% in pure oxygen for induction, 1.5% for maintenance during surgery and 0.8–1% during recording) and kept on a warming plate. The respiratory rate and the body temperature were continuously monitored and kept at 37 °C, 100–150 breaths per minute, respectively. Skin removal above V1 (−2.5 to −3.5 mm posterior to bregma and 2–3 mm lateral to midline) was performed after a subcutaneous injection of 2% lidocaine (Sanofi-Aventis, Frankfurt, Germany). The skull was thinned using a dental drill (NSK, Eschborn, Germany) and a custom-made recording chamber was fixed to the skull using cyanoacrylate glue (UHU, Bühl, Germany). Subsequently, the animal was moved into the imaging setup and the recording chamber was continuously perfused with warm (37 °C) artificial cerebrospinal fluid containing (in mM): 125 NaCl, 4.5 KCl, 26 $NaHCO_3$, 1.25 NaH_2PO_4, 2 $CaCl_2$, 1 $MgCl_2$, 20 glucose, pH 7.4 (when bubbled with 95% O_2 and 5% CO_2). A small craniotomy (≤0.5 mm) was performed above the V1 using a 30G needle. Neurons were labeled with a small molecule Ca^{2+} indicator Cal-520-AM (Tada et al., 2014) using the multi-cell bolus loading technique (Garaschuk et al., 2006; Stosiek et al., 2003). Briefly, the dye was dissolved in 20% Pluronic F-127 (Molecular Probes, Oregon, USA) solution (in DMSO) and was further diluted with a standard pipette solution (150 mM NaCl, 2.5 mM KCl, 10 mM HEPES (pH 7.4)), giving the final dye concentration of 0.5 mM. The solution was pressure-injected (70 kPa for 2 min) into the brain parenchyma approximately 150–200 µm below the dura. After one hour, the dye was fully taken up by neurons and astrocytes. Astrocytes could easily be distinguished from neurons by their bright appearance and cell-type-specific morphology.

2.1.3. Two-photon-imaging

Layer 2/3 neurons of the V1, located 150–190 µm below dura, were imaged in vivo using imaging system equipped with a custom-built two-photon microscope (Olympus Fluoview, Olympus) coupled to a mode-locked Ti-Sapphire laser working at 710–990 nm excitation wavelength (MaiTai, Spectra Physics), and a water-immersion objective (Nikon 40×, 0.8 NA). The excitation wavelength for Cal-520 was 800 nm. Spontaneous and visually-evoked Ca^{2+} signals were recorded at a frame rate of 7.7 Hz.

2.1.4. Drug application

400 µM Cyclopiazonic acid (CPA; Enzo Life Sciences, New York, USA) was added to the artificial cerebrospinal fluid perfusing the recording chamber ('bath application'). CPA was applied for 30 min prior to recording the drug effect. As we have recently shown, such treatment completely empties intracellular Ca^{2+} stores of layer 2/3 neurons (see Fig. 2 in (Lerdkrai et al., 2018)).

2.1.5. Visual stimulation

Visual stimuli were generated with the 'Psychtoolbox' (https://psychtoolbox.org/ HomePage) add-on package in Matlab (The Mathworks). The stimuli were projected onto a screen, which was placed 30 cm from the contralateral eye covering 80° x 60° of the visual field. Neurons were stimulated by the square-wave drifting gratings with 100% contrast, 0.03 cycles per degree and 1.5 Hz temporal frequency. The standard stimulation protocol started with a grey screen for 6 s (baseline condition), followed by static gratings for 6 s, a grey screen for 6 s and drifting gratings for 4 s. In each trial (6 trials in total)

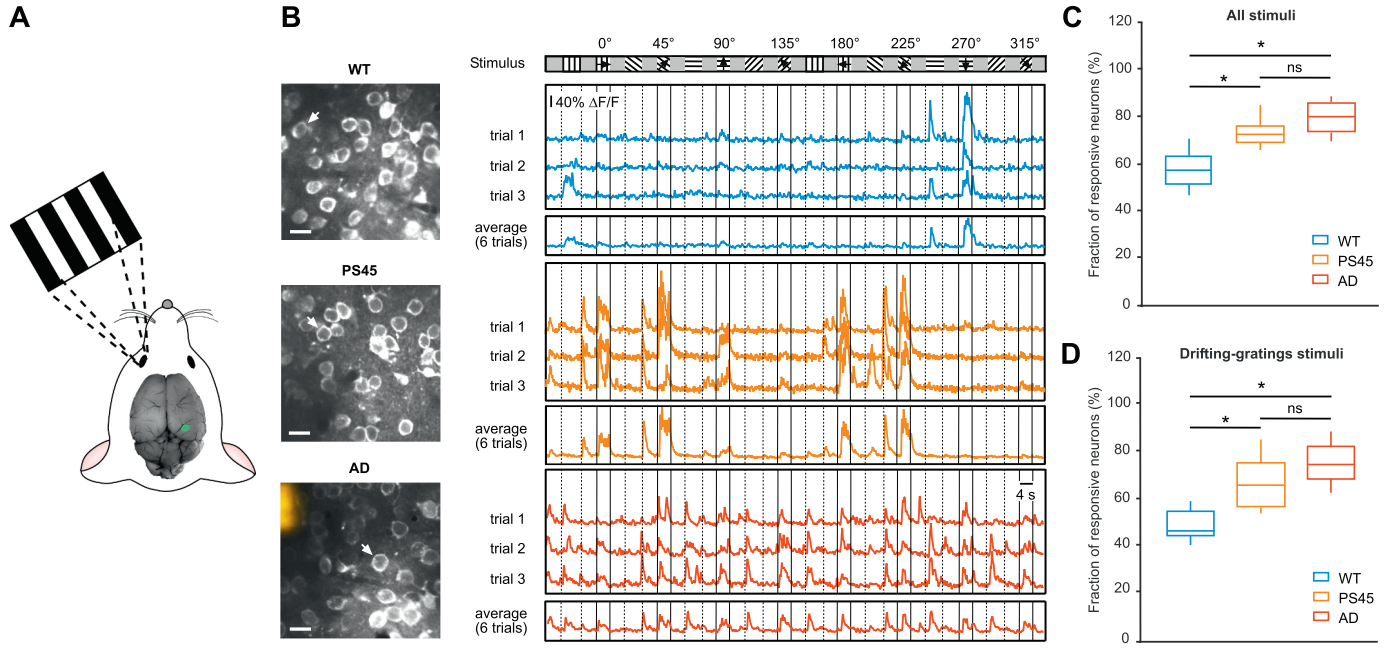

Fig. 1. Pathologically increased visual responsiveness in PS45 and AD mice. A, scheme of the experimental set up for two-photon Ca^{2+}-imaging of visually-evoked responses in cortical neurons. Layer 2/3 neurons of V1 were labeled using the Ca^{2+} indicator Cal-520 and static/drifting gratings were projected on a screen positioned 30 cm in front of the contralateral eye. B Left, maximum intensity projection (MIP) images of layer 2/3 neurons in V1 of a WT (top), a PS45 (middle) and an AD (bottom) mouse. Right, three representative traces and an average of six trials recorded from neurons marked with an arrowhead in the corresponding left panel, in response to standard stimulation protocol. C, box-and-whisker plot showing the fractions (per mouse) of neurons responding to any visual stimulus (i.e. either drifting or static ON/OFF gratings) in WT (blue), PS45 (orange) and AD (red) mice. Fraction of responsive neurons was significantly higher in PS45 and AD compared to WT mice ($p = .02$ for WT vs. PS45, $p < .01$ for WT vs. AD and $p = .28$ for PS45 vs. AD, Kruskal-Wallis test). D, box-and-whisker plot showing fractions (per mouse) of neurons responding to drifting gratings in WT (blue), PS45 (orange) and AD (red) mice. The fraction of responsive neurons was significantly higher in PS45 and AD compared to WT mice ($p = .03$ for WT vs. PS45, $p < .01$ for WT vs. AD and $p = .30$ for PS45 vs. AD, Kruskal-Wallis test). $n = 7, 6, 6$ mice for WT, PS45 and AD, respectively. Here and below, ΔF/F, relative change in fluorescence, ns, not significant; $^*p < .05$. (For interpretation of the references to colour in this figure legend, the reader is referred to the web version of this article.)

this protocol was repeated 8 times for 8 different directions of drifting gratings (see Fig. 1B). The start of the visual stimulation was synchronized with the start of the two-photon Ca^{2+} imaging.

2.1.6. Data analyses

Data analyses were performed offline with Image J (http://imagej.nih.gov/ij/), custom-made routines of Igor Pro (Wavemetrics) and MATLAB (The Mathworks). If not otherwise indicated, data is presented as median ± interquartile range. Lines of boxes represent 25th and 75th, and whiskers 10th and 90th percentiles.

For measurements of neuronal activity, we first read out the fluorescence intensity from regions of interest (ROIs) drawn around individual cell bodies and a background ROI, placed within a large blood vessel. Background-subtracted fluorescence intensity values were then used to calculate relative changes in fluorescence (ΔF/F) for individual neurons. A change in ΔF/F was considered as a Ca^{2+} transient when its amplitude was higher than threefold the standard deviation (SD) of the corresponding baseline noise. Baseline noise was computed by subtracting a strongly low pass filtered (moving average method) trace from the original signal. According to the frequency of their spontaneous Ca^{2+} transients, recorded neurons were classified as silent (0–0.25 transients/min), normal (0.26–4 transients/min) or hyperactive (> 4 transients/min) neurons (for details see (Busche et al., 2008; Lerdkrai et al., 2018)).

A neuron was considered visually responsive when the maximum ΔF/F of the averaged trace (mean of 6 trials) was higher than threefold the SD of the corresponding baseline noise. In addition, the main findings of the study were verified by using an alternative technique for identification of visually responsive neurons (as described in (Chen et al., 2013)). In the latter case (i) neuropil signal was estimated by averaging fluorescence signals of all pixels located outside the cell bodies (in ≥4 months old WT animals activity-dependent neuropil signal is generally negligible but might get larger in plaque-depositing AD mice (Busche et al., 2008)), (ii) $F_{cell\_measured}$ fluorescence signals were read out from ROIs drawn around individual cell bodies, (iii) the fluorescence signals of all cell bodies were corrected for a possible neuropil contamination by calculating $F_{cell\_true}(t) = F_{cell\_measured}(t) - 0.7 \times F_{neuropil}(t)$. Visually responsive neurons were defined as cells with significant stimulus-related fluorescence changes (ANOVA across presentation of the grey screen and either 8 directions of drifting gratings stimuli or 4 orientations of ON/OFF stimuli, $p < .01$, see also (Chen et al., 2013)). Please note that the second technique for identification of visually responsive neurons is less sensitive compared to the first one because of the higher noise of individual traces compared to the average trace.

In this study we measured neuron's responsiveness to 3 different kinds of visual stimuli: (i) drifting gratings, (ii) static gratings ON, measured during the beginning of the respective stimulus and (iii) static gratings OFF, measured 0–200 ms after switching off the respective stimulus. Direction and orientation selectivities were determined by direction (DSI) and orientation (OSI) selectivity indices (Niell and Stryker, 2008). The OSI is defined as $(R_{pref} - R_{ortho})/(R_{pref} + R_{ortho})$ and DSI is defined as $(R_{pref} - R_{opp})/(R_{pref} + R_{opp})$, where R_{pref} is the area under the ΔF/F transient recorded during the presentation of the preferred orientation or direction, respectively. R_{ortho} is the area under the ΔF/F transient recorded during the presentation of the orientation, orthogonal to R_{pref}. R_{opp} is the area under the ΔF/F transient recorded during the presentation of the direction, opposite to the preferred direction. Circular variance was calculated as $= 1 - \left|\frac{\sum R_k e^{2i\theta_k}}{\sum R_k}\right|$, where R_k is the area under the ΔF/F transient recorded during the presentation of drifting gratings at an angle θ_k, with θ_k ranging in our case from 0° to

360° in 45° steps (see also (Niell and Stryker, 2008)).

Activity ratio was calculated for each visually-responsive neuron by dividing the frequency of Ca^{2+} transients, recorded during the presentation of the grey screen (recording started 200 ms after grey screen ON and ended with grey screen OFF) by the frequency of Ca^{2+} transients, recorded before the presentation of the visual stimuli (i.e. during black screen).

2.1.7. Statistical analyses

For each experiment the choice of the sample size was based on biometrical sample size estimation. Statistics was performed using the GraphPad Prism 6 software (GraphPad Software, Inc.) and IBM SPSS Statistics (IBM Corporation). One-sample Kolmogorov-Smirnov test was used for assessing normality of data distribution. Two-sample Kolmogorov-Smirnov test was used for comparing two data distributions. Comparisons between two dependent variables were performed using the Wilcoxon-Signed-Rank test. Kruskal-Wallis test, followed by Dunn's post hoc test, was used for comparing three independent groups. Visually responsive neurons were identified using ANOVA. Two-way repeated measures ANOVA (rANOVA) with one between (mouse strains) and one within factor (control vs. treatment in the same animal) and F-tests followed by Fisher's LSD test was used for testing the effect of two independent factors within the same data set. In the regression analyses used for estimating the relationships between visual tuning properties (as measured by DSI, OSI, and circular variance) and the frequency of spontaneous activity, the dependency of measurements was adjusted for by Generalized Estimating Equations (GEE, (Zeger and Liang, 1986)), with exchangeable correlation structure. The values of the correlation coefficients given in the legend of Fig. 4 are purely descriptive, *p*-values refer to the GEE analysis. Differences were considered significant if $p < .05$.

3. Results

3.1. Heightened visual responsiveness in amyloid depositing mice

To study AD-related functional alterations of visual processing, layer 2/3 neurons in V1 of 10–12 months old WT, PS45 and AD mice were labeled with a small molecule Ca^{2+} indicator Cal-520 (Tada et al., 2014) using the multi cell bolus loading technique (Garaschuk et al., 2006; Stosiek et al., 2003). Visually-evoked Ca^{2+} transients in these neurons were caused by different visual stimuli (see below), projected on a screen placed at a 30 cm distance from the contralateral eye. A schematic of the experimental set up is shown in Fig. 1A. Fig. 1B shows three consecutive trials as well as the corresponding averaged traces, recorded from representative visually-responsive neurons (marked with an arrowhead on a respective left panel) in WT (top), PS45 (middle) and AD (bottom) mice.

Our visual stimulation protocol (Fig. 1B, top line) was designed to enable analyses of neuronal responses to different kinds of visual stimuli, including drifting gratings, static gratings ON and static gratings OFF stimuli. When analyzing the averaged traces, the fraction of layer 2/3 neurons responding to all kinds of visual stimuli in 10–12 months old WT mice was 57.3 ± 13.3% (Fig. 1C). Interestingly, the overall visual responsiveness in PS45 and AD mice was significantly higher, reaching 76.1 ± 8.5% and 79.7 ± 12.4%, respectively (Fig. 1C). Moreover, compared to WT mice, both PS45 and AD mice showed a significant increase in visual responsiveness to drifting gratings stimuli (Fig. 1D). In addition, in AD mice we observed a significantly increased fraction of neurons responding to static gratings ON (Fig. S1A) and static gratings OFF (Fig. S1B) stimuli. PS45 mice showed a similar trend but the observed difference did not reach the level of statistical significance (Fig. S1A, B).

Similar results were obtained when individual trials were used to identify visually responsive neurons (for details see Materials and methods section). The fraction of neurons responding to all kinds of visual stimuli in PS45 and AD mice was significantly higher (56.0 ± 16.2% for PS45 and 60.4 ± 19.1% for AD) compared to WT mice (36.4 ± 21.7%; $p = .02$ for WT vs. PS45, $p = .01$ for WT vs. AD and $p = .88$ for PS45 vs. AD, Kruskal-Wallis Test; $n = 7, 6, 6$ for WT, PS45 and AD, respectively). In addition, the fractions of neurons responding to drifting gratings stimuli in PS45 and AD mice (43.1 ± 10.4% for PS45 and 41.7 ± 7.5% for AD) were also significantly higher compared to those encountered in WT mice (27.9 ± 15.1%; p = .02 for WT vs. PS45, $p = .03$ for WT vs. AD and $p = .90$ for PS45 vs. AD, Kruskal-Wallis Test; n = 7, 6, 6 for WT, PS45 and AD, respectively).

Taken together, these results revealed an overall increase in visual responsiveness in 10–12 months old AD mice. Interestingly, a strong impairment of visual responsiveness was found also in PS45 mice, despite the lack of plaque deposition and neuroinflammation in this mouse strain (see Fig. S4 in Lerdkrai et al., 2018).

3.2. Differential impairment of visual tuning properties in PS45 and AD mice

Next, we calculated the area under the curve (AUC) of mean Ca^{2+} transients evoked by the preferred and non-preferred directions (Fig. 2A, B) as well as the preferred and non-preferred orientations (Fig. 2C, D) of drifting gratings stimuli. The visually responsive neurons in PS45 and AD mice had higher AUC of Ca^{2+} transients evoked by the non-preferred directions and non-preferred orientations than visually responsive neurons in WT mice (Fig. 2B, D). However, the AUCs of Ca^{2+} transients evoked by the preferred direction and orientation of drifting gratings stimuli in neurons of all three mouse strains were similar (Fig. 2A, C).

At the single cell level, layer 2/3 neurons of V1 in WT mice exhibit highly direction- and orientation-selective tuning, which can be described quantitatively by the direction (DSI) and orientation (OSI) selectivity indices (Niell and Stryker, 2008). To test whether visual tuning properties are changed in PS45 and AD mice, we compared DSI (Fig. 2E) and OSI (Fig. 2F) of visually responsive neurons in WT, PS45 and AD mice. The DSI of visually responsive neurons in PS45 and AD mice showed similar distributions on a population level, and the DSI distributions in both mouse strains were significantly shifted to lower values, compared to the DSI distribution in WT mice (Fig. 2E, left). When comparing AD and WT mice, a similar finding was observed when analyzing the distribution of the median DSI values per mouse (Fig. 2E, right). The median DSI value in PS45 mice was also smaller compared to that found in WT mice. This difference, however, did not reach the level of statistical significance. Furthermore, visually responsive neurons in AD mice had a significantly lower OSI, when compared with visually responsive neurons in WT mice (Fig. 2F). Interestingly, the visually responsive neurons in PS45 mice, despite exhibiting a decrease in the direction tuning (Fig. 2E), had orientation tuning largely similar to that of visually responsive neurons in WT mice (Fig. 2F).

The visually responsive neurons in AD mice (Fig. 2G, right) also showed a wider response function to oriented drifting gratings than visually responsive neurons in WT (Fig. 2G, left) and PS45 (Fig. 2G, middle) mice. To compare the response functions to oriented drifting gratings, we calculated the circular variance for all responses of each individual neuron. Visually responsive neurons from AD mice had significantly higher circular variances compared to those found in WT mice, whereas circular variances of visually responsive neurons in PS45 mice had intermediate values (Fig. 2H).

Taken together, these data revealed a profound impairment of tuning properties in AD mice. The latter included a significant decrease in DSI as well as OSI and a significant increase in the circular variance, likely caused by an increase in neuronal responsiveness to non-preferred directions/orientations stimuli. When considering the direction selectivity, the tuning properties of PS45 mice were similar to that of

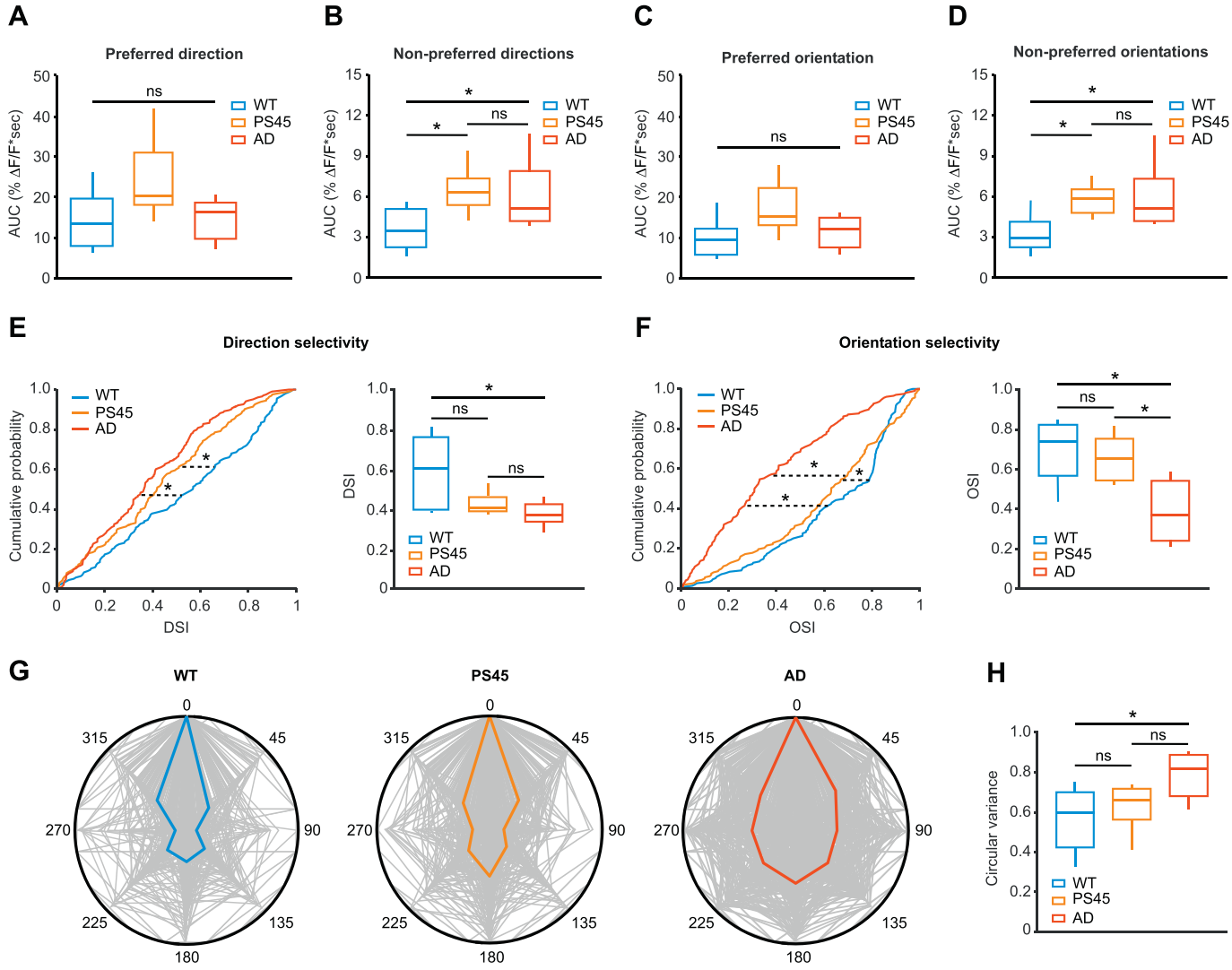

Fig. 2. Visual tuning properties are differentially affected in PS45 and AD mice. A-D, box-and-whisker plots showing the median (per mouse) areas under the curve (AUCs) of neuronal responses evoked by the preferred direction (A), non-preferred directions (B), preferred orientation (C) and non-preferred orientations (D) of drifting gratings stimuli in WT (blue), PS45 (orange) and AD (red) mice. There was no significant difference in AUCs of neuronal responses evoked by the preferred direction and the preferred orientation in WT, PS45 and AD mice ((A) $p = .08$, (C) $p = .09$, Kruskal-Wallis test). AUCs of neuronal responses evoked by non-preferred directions and non-preferred orientations in PS45 and AD mice were significantly higher compared to WT mice ((B) $p < .01$, for WT vs. PS45, $p < .05$, for WT vs. AD and $p = .44$ for PS45 vs. AD, Kruskal-Wallis test; (D) $p < .01$, for WT vs. PS45, $p = .04$ for WT vs. AD and $p = .57$ for PS45 vs. AD, Kruskal-Wallis test). E, F (left), cumulative probability functions showing the distributions of DSI (E) and OSI (F) of neurons in WT (blue), PS45 (orange) and AD (red) mice. Neurons in PS45 and AD mice had lower DSI compared to WT mice ($p < .01$ for both comparisons and $p = .08$ for PS45 vs. AD, Kolmogorov Smirnov test). Neurons in AD mice had lower OSI compared to WT and PS45 mice; neurons in PS45 mice had lower OSI compared to WT mice ($p < .01$ for all comparisons, Kolmogorov Smirnov test). E, F (right), box-and-whisker plots showing the median (per mouse) DSI (E) and OSI (F) in WT (blue), PS45 (orange) and AD (red) mice. The median DSI in AD mice was lower compared to WT mice ($p < .01$ for WT vs. AD, $p = .11$ for WT vs. PS45 and $p = .33$ for PS45 vs. AD, Kruskal-Wallis test), and the median OSI in AD mice was lower compared to WT and PS45 mice ($p < .01$ for WT vs. AD, $p = .03$ for PS45 vs. AD and $p = .66$ for WT vs. PS45, Kruskal-Wallis test). G, polar plots showing response functions of all neurons (grey) to oriented drifting gratings in WT, PS45 and AD mice. The medians of neuronal responses in WT, PS45 and AD mice are shown as blue, orange and red lines, respectively. H, box-and-whisker plot showing the median (per mouse) circular variance in WT (blue), PS45 (orange) and AD (red) mice. Circular variance increased in AD mice, compared to WT mice ($p = .01$ for WT vs. AD, $p = .56$ for WT vs. PS45 and $p = .07$ for PS45 vs. AD, Kruskal-Wallis test). WT: $n = 156$ neurons, 7 mice; PS45: $n = 163$ neurons, 6 mice; AD: $n = 203$ neurons, 6 mice. (For interpretation of the references to colour in this figure legend, the reader is referred to the web version of this article.)

AD mice, but when considering orientation selectivity and the circular variance, they were more similar to that of WT mice.

3.3. Relationship between the degree of visual impairment and the frequency of ongoing neuronal activity

In the AD mouse strain used in this study, the impairment of the orientation selectivity was previously reported to occur selectively in hyperactive neurons (Grienberger et al., 2012). Therefore, next we analyzed the correlation between the frequency of spontaneous activity in individual neurons and their visual tuning properties. To do so, the frequency of spontaneous Ca^{2+} transients of a respective neuron was measured first during the presentation of a dark screen. Thereafter, we ran our usual stimulation protocol (Fig. 1B), to determine the neuron's DSI, OSI and the circular variance.

Fig. 3A shows representative recordings of spontaneous Ca^{2+} transients from neurons in WT (top, here and below the recorded neurons are marked with respective numbers in the left panel), PS45 (middle) and AD (bottom) mice. Similar to our previous findings in the frontal/motor cortex (Lerdkrai et al., 2018), the frequency distributions

of spontaneous Ca^{2+} transients recorded in V1 of PS45 and AD mice were significantly shifted to higher frequencies, compared to the frequency distribution found in WT mice (Fig. 3B). The median (per mouse) frequencies of spontaneous Ca^{2+} transients in PS45 and AD mice were also significantly higher, compared to that found in WT mice (Fig. 3C).

For a direct comparison of our findings with the previous study (Grienberger et al., 2012), we classified all recorded neurons as silent, normal and hyperactive based on the frequency of their spontaneous Ca^{2+} transients (the frequency ranges are given in the Materials and methods section, the same analyses as in (Busche et al., 2008; Grienberger et al., 2012; Lerdkrai et al., 2018)) and compared the tuning properties of normal and hyperactive neurons in the three mouse strains. In contrast to what was found in younger AD mice, in which the

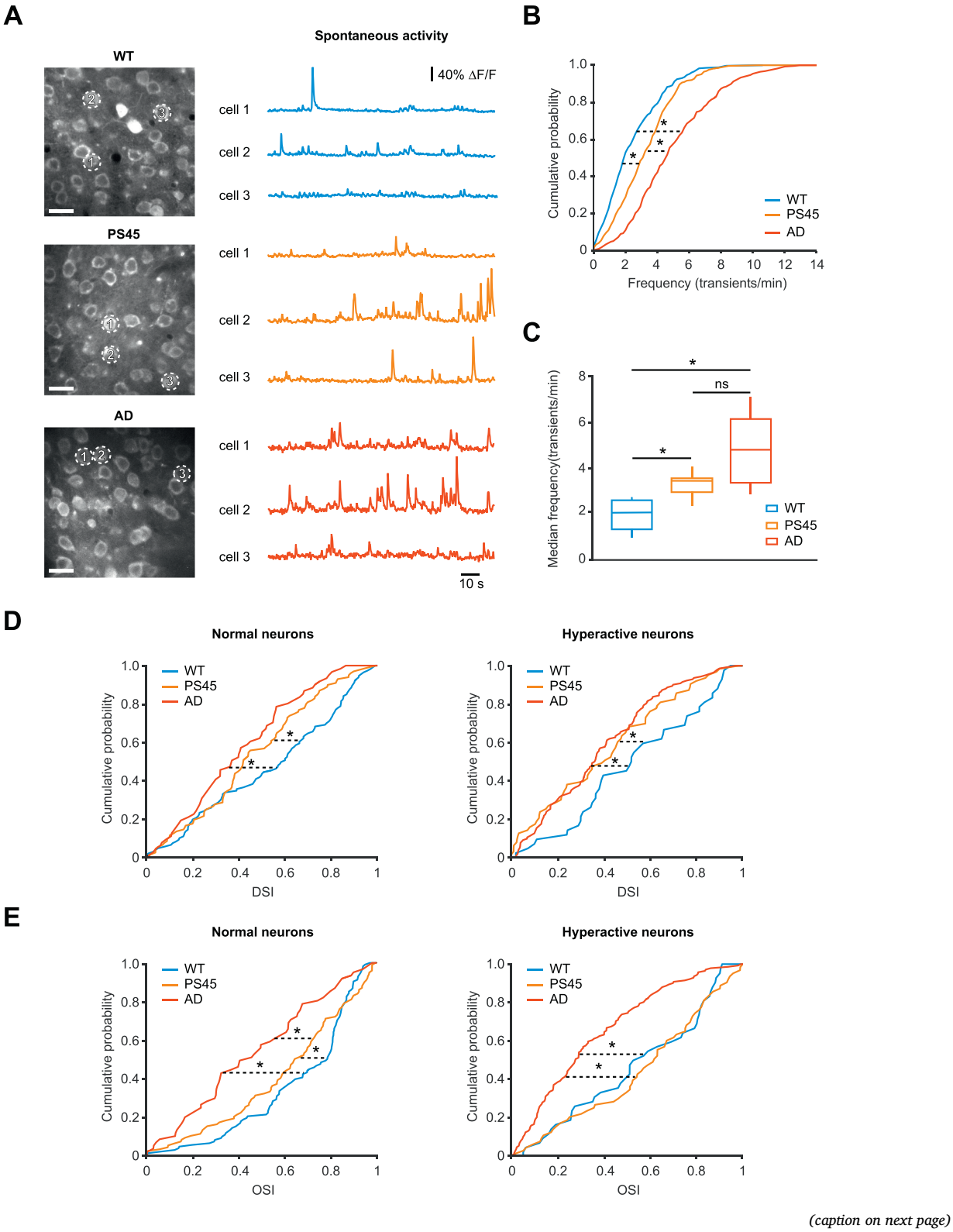

(caption on next page)

Fig. 3. Visual tuning properties are impaired in both normal and hyperactive neurons. A left, MIP images of layer 2/3 neurons in a WT (top), a PS45 (middle) and an AD (bottom) mouse. Scale bars represent 10 μm. Right, spontaneous Ca^{2+} transients recorded simultaneously from neurons marked with respective numbers in the corresponding left panel. B, cumulative probability functions showing frequency distributions of spontaneous Ca^{2+} transients in WT (blue), PS45 (orange) and AD (red) mice. The frequency distributions in PS45 and AD mice are significantly shifted towards higher frequencies compared to WT mice ($p < .01$ for all comparisons, Kolmogorov Smirnov test). C, box-and-whisker plot showing the median (per mouse) frequency of spontaneous Ca^{2+} transients in WT (blue), PS45 (orange) and AD (red) mice. The median frequencies in PS45 and AD mice are significantly higher compared to WT mice ($p = .03$ for WT vs. PS45, $p < .01$ for WT vs. AD and $p = .22$ for PS45 vs. AD, Kruskal-Wallis test). D, E, cumulative probability functions showing the distributions of DSI of normal (D, left) and hyperactive (D, right) neurons and OSI of normal (E, left) and hyperactive (E, right) neurons in WT (blue), PS45 (orange) and AD (red) mice. In normal and hyperactive neurons of PS45 and AD mice the distributions of DSI are significantly shifted towards the lower values compared to respective distributions recorded in WT mice (D, left: $p = .03$ for WT vs. PS45, $p < .01$ for WT vs. AD and $p = .16$ for PS45 vs. AD, Kolmogorov Smirnov test; D, right: $p = .04$ for WT vs. PS45, $p = .01$ for WT vs. AD and $p = .60$ for PS45 vs. AD, Kolmogorov Smirnov test). The distributions of OSI of normal and hyperactive neurons recorded in AD mice are significantly shifted towards the lower values compared to WT and PS45 mice and the distribution of OSI in normal neurons of PS45 mice is slightly but significantly shifted towards lower OSI compared to the respective distribution recorded in WT mice (E, left: $p < .01$ for all comparisons, Kolmogorov Smirnov test; E, right: $p = .65$ for WT vs. PS45, $p < .01$ for WT vs. AD, $p < .01$ for PS45 vs. AD, Kolmogorov Smirnov test). Normal neurons, WT: $n = 110$ neurons, 7 mice; PS45: $n = 99$ neurons, 6 mice; AD: $n = 61$ neurons, 6 mice; Hyperactive neurons, WT: $n = 42$ neurons, 7 mice; PS45: $n = 63$ neurons, 6 mice; AD: $n = 142$ neurons, 6 mice. (For interpretation of the references to colour in this figure legend, the reader is referred to the web version of this article.)

AD-related functional impairment was restricted to the hyperactive cells only (Grienberger et al., 2012), both normal and hyperactive cells showed the impairment of visual tuning properties in 10–12 months old PS45 and AD mice (Fig. 3D, E), virtually repeating findings presented in Fig. 2E, F for the entire neuronal population.

Correlations between the frequencies of spontaneous Ca^{2+} transients and the visual tuning properties (DSI, OSI and circular variance) of a neuron were calculated using GEE analysis (for details see Materials and methods section). There was no correlation between DSI and the frequency of spontaneous Ca^{2+} transients in visually responsive neurons of WT, PS45 and AD mice (Fig. 4A-C). However, there was a significant correlation between OSI and the frequency of spontaneous Ca^{2+} transients in visually responsive neurons of all three mouse strains (Fig. 4D-F). Similar to OSI, circular variance of neuronal responses in WT (Fig. 4G) and AD (Fig. 4I) mice was significantly correlated with the frequency of spontaneous Ca^{2+} transients in these neurons. In neurons from PS45 mice (Fig. 4H) there also was a trend towards such a correlation. However, the correlation coefficient in this case did not reach the level of statistical significance.

Altogether, these data documented the presence of neuronal hyperactivity in the visual cortex of both PS45 and AD mouse strains and revealed a linear relationship between the frequency of ongoing neuronal activity and the degree of impairment of their orientation selectivity and, to a lesser extent, the circular variance of their visual responses on a single cell level. On the population level, however, both normal and hyperactive neurons of the 10–12 months old PS45 and AD mice showed a significant impairment of the visual tuning properties.

3.4. Visually-evoked suppression of spontaneous activity is impaired in AD mice

When conducting the imaging protocol described above (Fig. 1B), we noticed that in WT mice spontaneous Ca^{2+} transients, abundant during the presentation of a dark screen, almost disappeared during the visual stimulation (compare Fig. 3A with Fig. 1B). Hence, we measured the frequency of spontaneous Ca^{2+} transients during the intermittent resting periods while presenting visual stimuli (grey screen presentation, see Fig. 1B) and compared it with the frequency of spontaneous Ca^{2+} transients measured in the same neuron before the presentation of the visual stimuli (dark screen presentation, as in Fig. 3A). The analyses of these data (Fig. 5) revealed a clear suppression of spontaneous activity by visual stimuli in visually responsive neurons of WT (Fig. 5A), and PS45 (Fig. 5B) mice. In AD mice, however, the suppression was much less prominent (Fig. 5C). To quantify our observations, we calculated the ratio between the frequencies of Ca^{2+} transients recorded before and during the presentation of the visual stimuli (Activity ratio). In WT mice (Fig. 5D), the median (per mouse) activity ratio was 0.49 ± 0.32, documenting a clear suppression of spontaneous activity by visual stimuli. The neurons in PS45 mice showed a similar median activity ratio (0.47 ± 0.16), whereas the median activity ratio in AD mice (0.71 ± 0.27) was significantly higher, documenting a clear lack of suppression of spontaneous activity by visual stimuli in this mouse strain (Fig. 5D).

Taken together, these data revealed that visually-responsive neurons in WT and PS45 mice exhibit a strong sensory stimulus-induced suppression of the spontaneous activity and that this suppression was impaired in AD mice.

3.5. Calcium store depletion reduced neuronal hyperactivity in both PS45 and AD mouse strains

Because the impairment of the orientation selectivity and the circular variance of visual responses turned out to be correlated with the degree of neuronal hyperactivity, we tested whether reducing neuronal hyperactivity in PS45 and AD mice can reverse the observed impairment of visual processing. To do so, we topically applied CPA to the cortical surface. This treatment was shown to reduce neuronal hyperactivity in layer 2/3 neurons of the frontal/motor cortex in PS45 and AD mice (Lerdkrai et al., 2018).

First, we tested whether CPA reduces neuronal hyperactivity also in V1 of PS45 and AD mice. To this end, the frequency of spontaneous Ca^{2+} transients of layer 2/3 neurons was recorded before and during the application of 400 μM CPA (30-min-long pretreatment; this protocol completely abolishes caffeine-induced Ca^{2+}release from the intracellular Ca^{2+} stores in layer 2/3 neurons in vivo (Lerdkrai et al., 2018)). CPA application reduced the fraction of hyperactive neurons in AD mice from 58% to 37% and increased the fraction of normal neurons from 40% to 60% (Fig. 6A). A similar effect was also observed in PS45 mice. At the level of the entire population CPA significantly reduced the frequency of spontaneous Ca^{2+} transients in PS45 and AD mice, without affecting the frequency of spontaneous Ca^{2+} transients in WT mice (Fig. 6B-E).

These data show that neuronal hyperactivity in V1 of PS45 and AD mice is also caused (at least in part) by the dysfunction of intracellular Ca^{2+} stores and document the ability of CPA to reduce the AD-mediated neuronal hyperactivity in this brain area.

3.6. Role of Ca^{2+} store-mediated neuronal hyperactivity for the impairment of visual response properties in PS45 and AD mice

In the next series of experiments, we tested whether reducing neuronal hyperactivity in PS45 and AD mice can counteract the impairment of visual response properties. First, we tested whether the presence of CPA changes the fraction of visually-responsive neurons, which is considerably increased in PS45 and AD mice (Fig. 1C, D). As shown in Fig. 7A, B, CPA significantly reduced pathologically increased visual responsiveness to all visual stimuli and to drifting gratings stimuli both in PS45 and AD mice, without changing visual responsiveness in WT

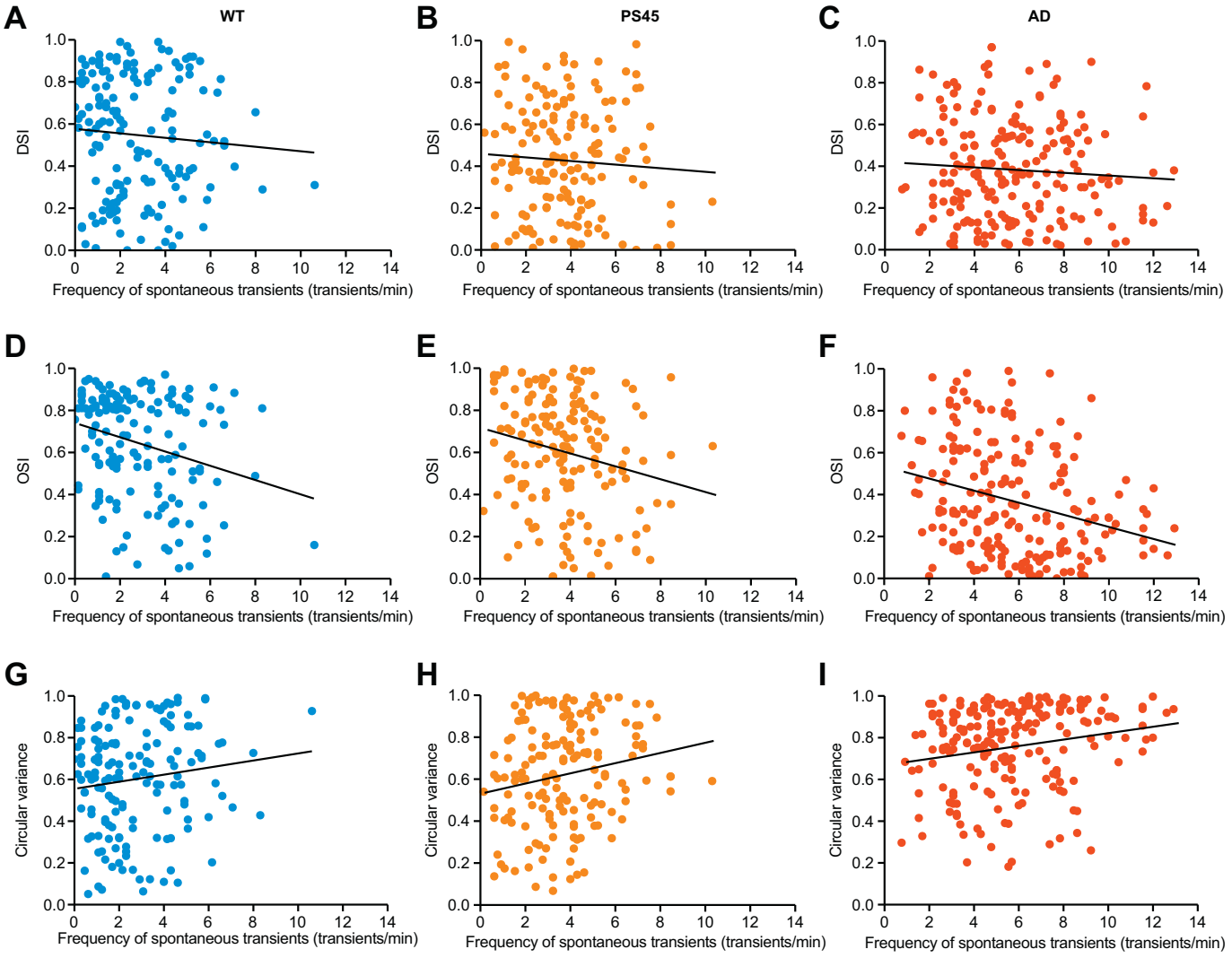

Fig. 4. The degree of visual impairment correlates with the degree of neuronal hyperactivity. A-C, scatter plots illustrating the relationship between the frequency of spontaneous Ca^{2+} transients and DSI of all visually responsive neurons in WT (A), PS45 (B) and AD (C) mice. There is no correlation between the frequency of spontaneous Ca^{2+} transients and DSI in all mouse lines tested ($p = .91$, $R = 0.04$ for WT, $p = .20$, $R = -0.06$ for PS45 and $p = .63$, $R = -0.07$ for AD mice, GEE). D-F, scatter plots illustrating the relationship between the frequency of spontaneous Ca^{2+} transients and OSI of all visually responsive neurons in WT (D), PS45 (E) and AD (F) mice. Visually responsive neurons in all mouse lines show negative correlation between the frequency of spontaneous Ca^{2+} transients and OSI ($p < .01$, $R = -0.27$ for WT, $p < .01$, $R = -0.22$ for PS45 and $p = .03$, $R = -0.29$ for AD mice, GEE). G-I, scatter plots illustrating the relationship between the frequency of spontaneous Ca^{2+} transients and the circular variance of all visually responsive neurons in WT (G), PS45 (H) and AD (I) mice. Visually responsive neurons in WT and AD mice show a positive correlation between the frequency of spontaneous Ca^{2+} transients and the circular variance ($p < .01$, $R = 0.13$ for WT, $p = .06$, $R = 0.19$ for PS45 and $p = .03$, $R = 0.20$ for AD mice, GEE). WT: n = 156 neurons, 7 mice; PS45: n = 163 neurons, 6 mice; AD: n = 203 neurons, 6 mice.

mice. Actually, under CPA the fractions of visually-responsive neurons in PS45 and AD mice were not significantly different from those in WT mice under control conditions ($p = .34$ for all visual stimuli and $p = .36$ for drifting gratings stimuli, Kruskal-Wallis test; $n = 5, 6, 6$ mice for WT, PS45 and AD, respectively). Similar results were obtained when analyzing only neurons identified as visually responsive based on individual trials (all visual stimuli: $p = .63$ for WT, $p = .03$ for PS45 and $p = .03$ for AD; drifting gratings stimuli: $p = .99$ for WT, $p = .03$ for PS45 and $p = .03$ for AD, Wilcoxon Signed-Rank test;. n = 5, 6, 6 mice for WT, PS45 and AD, respectively). Further, we tested whether CPA can recover the sensory stimulus-induced suppression of spontaneous activity (Fig. 5) in AD mice. However, the activity ratios before and during CPA application in WT, PS45 and AD mice remain the same ($p = .5$ for WT, $p = .22$ for PS45 and $p = .42$ for AD mice, Wilcoxon-Signed-Rank test; n = 5, 6, 6 mice for WT, PS45 and AD, respectively).

Next, we analyzed the visual tuning properties before and during the application of CPA. Polar plots (Fig. S2A) illustrate the effect of CPA on neuronal responses to oriented drifting gratings in WT (left), PS45 (middle) and AD (right) mice. Unexpectedly, the reduction of neuronal hyperactivity by CPA in PS45 and AD mice had no effect on the DSI, OSI and circular variance of neuronal responses both on a single cell level (Fig. S3) and when analyzing the median effect per mouse (Fig. S2B-D).

In summary, these data suggest that Ca^{2+} store-mediated neuronal hyperactivity contributes to a pathological increase of visual responsiveness in PS45 and AD mice. The latter can thus be ameliorated by emptying of the intracellular stores by CPA. At the same time, the stimulus-induced suppression of spontaneous activity and the impairment of visual tuning properties likely rely on different cellular/molecular mechanisms, which remain to be elucidated.

4. Discussion

This study represents one of the most complete analyses of the visual response properties in a mouse model of AD. It documents a

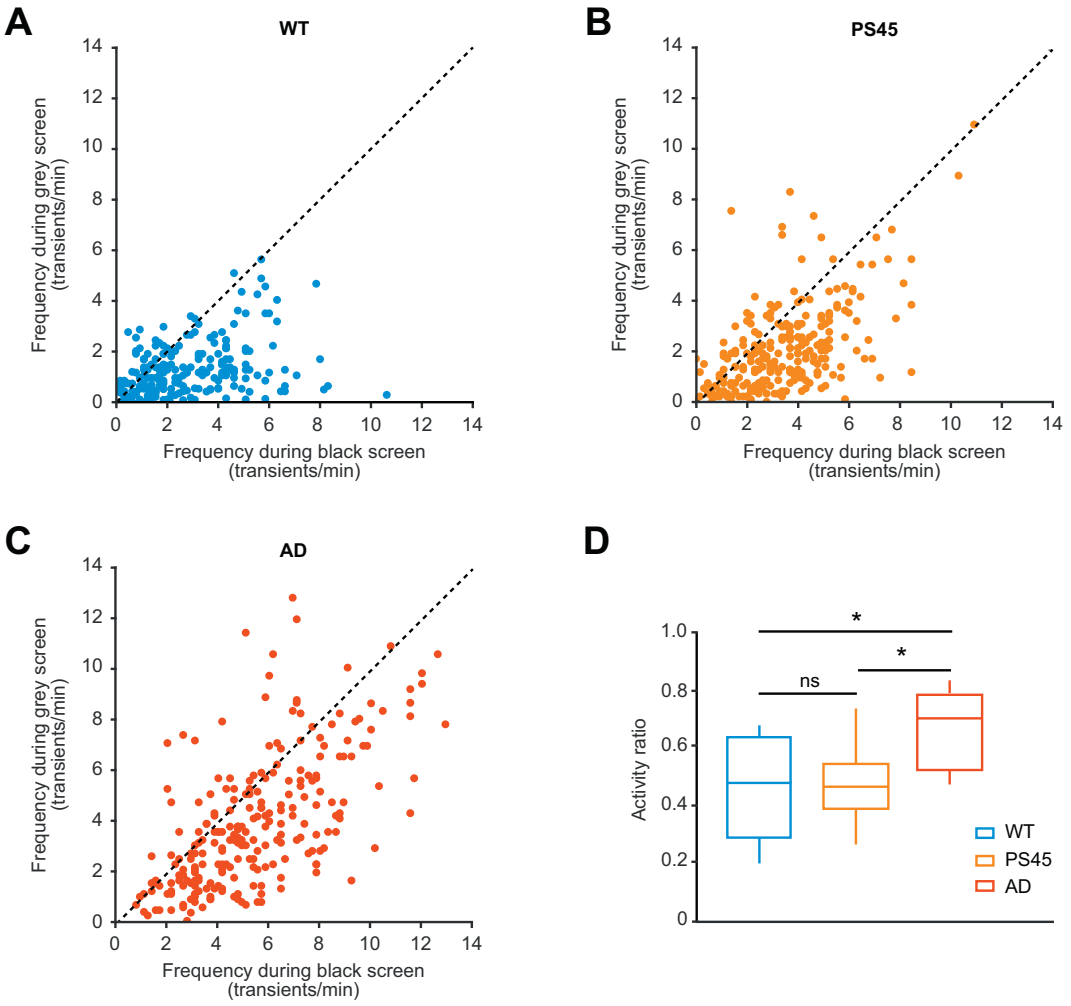

Fig. 5. Impairment of the stimulus-induced suppression of spontaneous activity in AD mice. A-C, scatter plots illustrating the relationship between the frequency of spontaneous transients during the presentation of the black screen (X-axis) and the grey screen (Y-axis) for all visually responsive neurons in WT (A), PS45 (B) and AD (C) mice. D, box-and-whisker plot showing the median (per mouse) activity ratios for all visually responsive neurons of WT (blue), PS45 (orange) and AD (red) mice. The stimulation-induced suppression of spontaneous Ca^{2+} transients is significantly impaired in AD compared to WT and PS45 mice ($p = .04$ for WT vs. AD, $p = .02$ for PS45 vs. AD and $p = .72$ for WT vs. PS45, Kruskal-Wallis test). $n = 7, 6, 6$ mice for WT, PS45 and AD, respectively. (For interpretation of the references to colour in this figure legend, the reader is referred to the web version of this article.)

significant impairment of visual processing in AD mice including (i) an overall increase in visual responsiveness, (ii) a profound decline of visual tuning properties and (iii) an impairment of the stimulus-induced suppression of spontaneous activity. Moreover, the degree of the impairment of visual tuning correlated with the level of neuronal activity. Interestingly, some (e.g. an overall increase in visual responsiveness, a decrease in direction selectivity) but not all of these alterations were found in PS45 mice devoid of amyloid deposition and neuroinflammation (Fig. S4 in Lerdkrai et al., 2018), suggesting that these aspects of visual impairment are solely caused by a G384A mutation in a single allele of the presenilin 1 gene. We further show that an increased visual responsiveness in PS45 and AD mice is mainly caused by a dysfunction of the intracellular Ca^{2+} stores because it can be normalized by CPA-mediated store depletion.

This study was conducted using a novel small molecule Ca^{2+} indicator Cal-520, reported to yield Ca^{2+} transients of larger amplitudes and higher signal-to-noise ratios compared to the commonly used Oregon Green BAPTA 1 (Tada et al., 2014). Despite these advantages of Cal-520, the fractions of visually-responsive neurons, measured in the current study, were similar to those observed by others (e.g. (Chen et al., 2013)) with Oregon Green BAPTA 1 or GCaMP6f.

By studying the same animal model of AD at a more advanced age, our data are directly comparable with the study conducted by Arthur Konnerth's group (Grienberger et al., 2012). Our data are consistent with the strong impairment of the orientation and a somewhat weaker impairment of the direction tuning found by the colleagues in 8–10 months old $APP_{SWE}/PS1_{G384A}$ mice. However, whereas the fractions of visually-responsive cells were similar in 8–10 months old WT and AD mice (Grienberger et al., 2012), at the age studied here (10–12 months) a significantly larger fraction of cells in AD mice became visually-responsive (Fig. 1). Thus, our study is the first to reveal an AD-related increase in the number of visually-responsive cells in the mammalian primary visual cortex. This increase was largely independent of the precise nature of the visual stimuli but turned out to be somewhat stronger in AD compared to PS45 mice (Fig. 1C, D and Fig. S1A, B). Because of the CPA sensitivity of this phenomenon and its presence in the heterozygous PS45 mice, we conclude that it is most probably caused by the heightened Ca^{2+} store-dependent release of an excitatory neurotransmitter (likely glutamate) from the presynaptic terminals. This observation adds a new facet to our knowledge about the neural network dysfunction in AD by showing that not only the spontaneous ongoing activity (Lerdkrai et al., 2018) but also the responses to sensory stimuli are potentiated by the AD-related mutation in the PS1 gene. As the modern human life is full of flickering photic

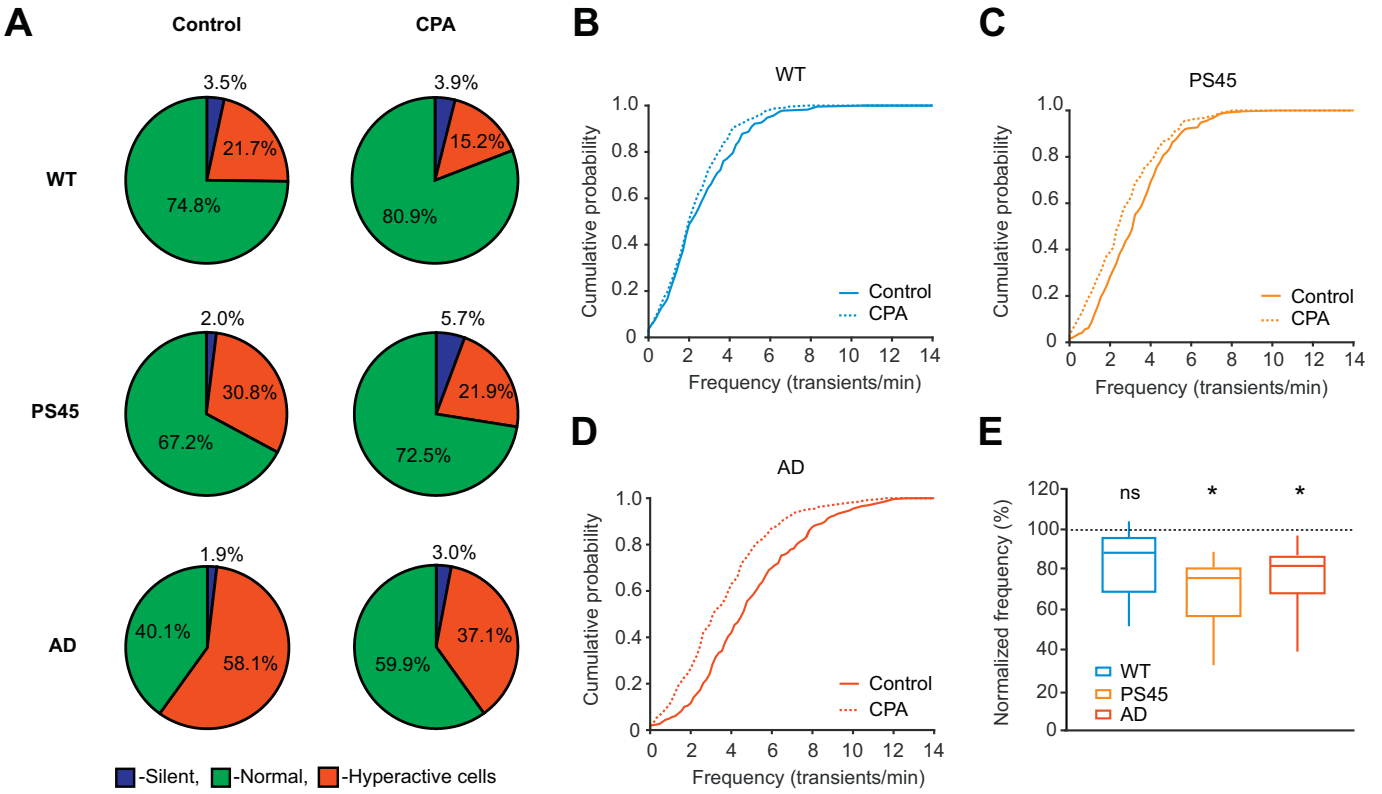

Fig. 6. Store depletion reduced neuronal hyperactivity in both PS45 and AD mice. A, pie charts illustrating the fractions of silent (blue), normal (green) and hyperactive (red) neurons before (Control) and during the application of CPA (CPA) in WT (top), PS45 (middle) and AD (bottom) mice. B-D, cumulative probability functions showing the frequency distributions of spontaneous Ca^{2+} transients before (Control) and during the application of CPA (CPA) in WT (B), PS45 (C) and AD (D) mice. E, box-and-whisker plot showing the effect of CPA on the frequency of spontaneous Ca^{2+} transients in WT (blue), PS45 (orange) and AD (red) mice. Data are shown as median (per mouse) values under CPA normalized to the respective control values. The frequency of spontaneous Ca^{2+} transients significantly decreased under CPA in PS45 and AD mice ($p < .01$ for PS45, $p = .01$ for AD and $p = .08$ for WT, two-way rANOVA). $n = 5, 6, 6$ mice for WT, PS45 and AD, respectively. (For interpretation of the references to colour in this figure legend, the reader is referred to the web version of this article.)

stimuli (e.g. generated by TVs, computer games and electronic instruments with flickering displays) it is likely that in addition to causing exaggerated responses to visual stimuli, the PS1-related increase in visual responsiveness is also decreasing the threshold for induction of photically triggered synchronized neuronal discharges or even seizures (Martins Da Silva and Leal, 2017).

According to data presented here ageing of WT, PS45 and AD mice is paralleled by an overall increase of neuronal hyperactivity in the visual cortex (compare Fig. 6 with Supplementary Fig. S6 of (Grienberger et al., 2012)). Indeed, at around one year of age the fraction of hypoactive/silent cells seems to decrease dramatically and from now on neuronal network hyperactivity seems to represent the functional impairment of the ageing brain. Although clearly seen already during normal ageing (Fig. 6, see also (Lerdkrai et al., 2018)), neuronal network hyperactivity is even higher in AD mice and an increase in neuronal activity correlates significantly with a decrease in orientation selectivity and an increase in circular variance of visually responsive neurons (Fig. 4). Our study is also the first to describe the impairment of visual response properties in PS45 mice, as at younger age they were found to be asymptomatic (Grienberger et al., 2012). Moreover, in contrast to the data obtained by others (Grienberger et al., 2012), normal cells of AD mice studied here also had strongly impaired orientation and direction selectivity (Fig. 3D, E). Taken together, our data add one more stage to the description of the stage-specific decline of the visual response properties in this mouse model of AD. This stage is characterized by a strong increase in the fraction of hyperactive cells, virtual disappearance of neuronal hypoactivity, an overall increase in visual responsiveness in AD compared to WT mice and an extension of the impairment of visual tuning properties onto an entire neuronal population (including normal and hyperactive cells) in AD mice.

Using another mouse model of AD ($APP_{SWE}/PS1_{L166P}$ mice) Liebscher et al. (Liebscher et al., 2016) could not observe any impairment of the visual response properties in 10–11 months old mice, despite the presence of substantial neuronal hyperactivity. The reason for this discrepancy remains unknown. One obvious difference is that their mice harbored another mutation in the presenilin gene, which might endow neurons with different functional properties. Although experiments of Liebscher et al. were conducted in awake and ours as well as those of A. Konnerth's group (Grienberger et al., 2012) in anesthetized mice, this experimental difference is unlikely to account for the mentioned above discrepancy because the impairment of the visual processing was also present in awake $APP_{SWE}/PS1_{G384A}$ mice. Indeed, these mice were unable to discriminate drifting gratings of two different orientations separated by 22.5° (Grienberger et al., 2012). Moreover, Niell & Stryker reported similar orientation selectivity and tuning width of mouse layer 2/3 neurons recorded in awake state and under anesthesia (Niell and Stryker, 2010).

What are the possible mechanisms underlying the described above impairment of the visual response properties? The impairment of the direction selectivity in PS45 mice presenting with neuronal hyperactivity but not with amyloidosis and neuroinflammation (Fig. 2), the lack of inhibition of spontaneous activity during the presentation of visual stimuli in AD mice (Fig. 5), the overall increase in visual responsiveness in PS45 and AD compared to WT mice (Fig. 3), and the correlation between the degree of visual impairment and that of neuronal hyperactivity on a single cell level (Fig. 4) all pointed to neuronal hyperactivity as the main cause of deterioration of visual response properties in AD mice. However, a significant reduction of neuronal

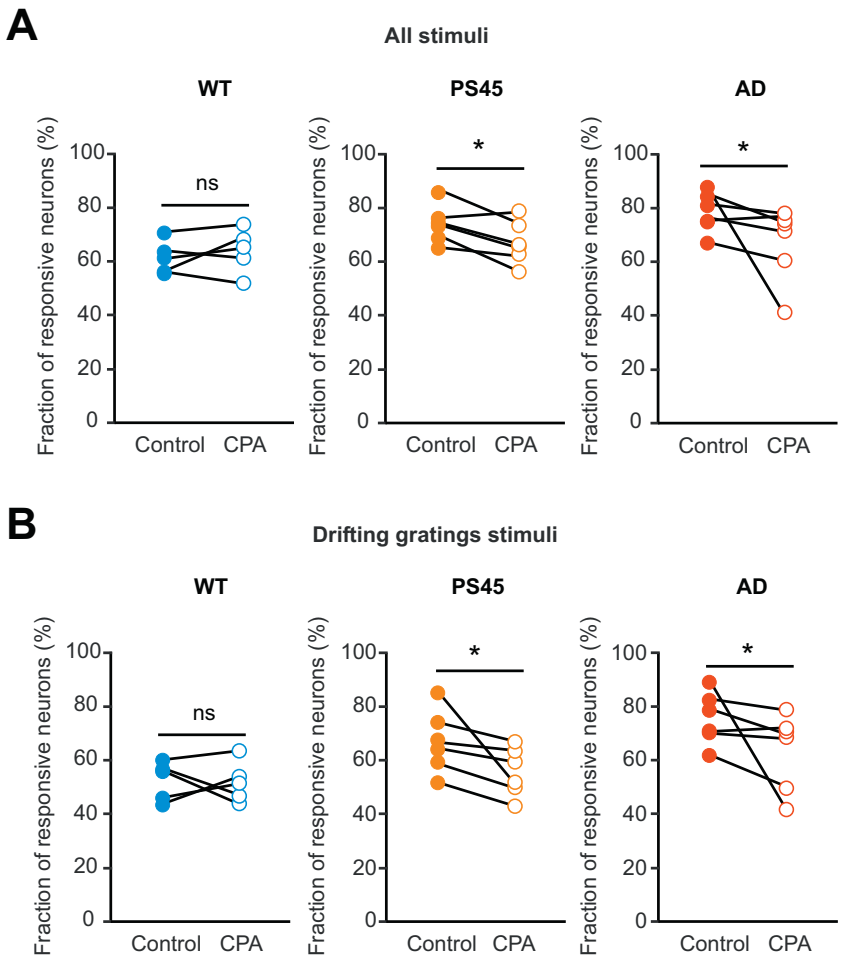

Fig. 7. Store depletion ameliorates the pathological increase in visual responsiveness. A-B, dot plots showing the effect of CPA-mediated store blockade on the fractions of visually responsive neurons in WT (blue), PS45 (orange) and AD (red) mice. CPA reduced the fractions of neurons responding to all visual stimuli (A) and drifting gratings stimuli (B) in PS45 and AD mice without affecting responses in WT mice ((A) $p = .41$ for WT, $p = .046$ for PS45 and $p = .03$ for AD, Wilcoxon Signed-Rank test; (B) $p = .41$ for WT, $p = .02$ for PS45 and $p = .03$ for AD, Wilcoxon Signed-Rank test), $n = 5, 6, 6$ mice for WT, PS45 and AD, respectively. (For interpretation of the references to colour in this figure legend, the reader is referred to the web version of this article.)

hyperactivity by emptying the intracellular Ca^{2+} stores improved some but not all aspects of AD-related visual dysfunction. The store depletion normalized the exaggerated visual responsiveness in PS45 and AD mice (Fig. 7) but the visual tuning properties still remained impaired.

If not neuronal hyperactivity, which mechanisms might contribute to the impairment of visual tuning properties in AD mice? The use of PS45 mice revealed dissociation between the impairment of the direction and the orientation selectivity. Although the overall degree of impairment of the direction selectivity in AD mice was smaller than that of the orientation selectivity (Fig. 2), only the former was seen in PS45 mice. This data allows to exclude (i) accumulation of fibrillar amyloid β species, (ii) activation of astrocytes and microglia, (iii) neuronal hyperactivity as well as (iv) AD-related aggregation of tau protein in neurofibrillary tangles (Kuchibhotla et al., 2014) from the mechanisms underlying the impairment of the direction selectivity in AD mice. As for the impairment of orientation selectivity, the latter is more likely to be mediated via mechanisms triggered by amyloidosis or neuroinflammation. We suggest that one of such mechanisms might involve the dysfunction of parvalbumin-positive (PV^+) inhibitory interneurons, initially observed in hAPP mice (Verret et al., 2012). Indeed, modulating spiking activity of PV^+ interneurons was recently shown to influence visual tuning properties of pyramidal neurons in the V1 (Atallah et al., 2012; Lee et al., 2012). Specifically, an acute optogenetically-induced excitation of PV^+ neurons caused a significant increase in the orientation and direction selectivity of layer 2/3 cells in awake as well as anesthetized state (Atallah et al., 2012; Lee et al., 2012), whereas a selective inhibition of PV^+ cells had an opposite effect (Atallah et al., 2012).

Another important result of our study is the discovery of the visual stimulation-induced inhibition of the ongoing spontaneous activity and of the impairment of this inhibition in a mouse model of AD. Together with the recent observation in the rat barrel cortex, where single or repetitive whisker deflections were also shown to inhibit the ongoing neuronal activity (Deneux and Grinvald, 2017), this finding identifies a general mechanism of interplay between the sensory-driven and spontaneous ongoing activities. This interplay appears to be bidirectional in nature, with ongoing spontaneous activity influencing the strength of sensory-evoked responses (Petersen et al., 2003) and vice versa, sensory-evoked responses influencing the ongoing spontaneous activity (this study and (Deneux and Grinvald, 2017)). In the barrel cortex sensory stimulation reduced firing of 57% of recorded neurons but increased firing of 7% of recorded cells (Deneux and Grinvald, 2017). We propose that the latter cells are parvalbumin- or somatostatin-expressing interneurons, inhibiting the surrounding pyramidal cells. In a mouse model of AD, a PS1-mutation independent dysfunction of these inhibitory neurons (Schmid et al., 2016; Verret et al., 2012) is likely responsible for the lack of sensory-driven inhibition and the heightened ongoing activity during the presentation of the visual stimuli (Fig. 5). This interfering ongoing activity is very likely to decrease decoding accuracy of V1 pyramidal neurons (Liebscher et al., 2016) causing AD-related deficits in visual discrimination in mice (Grienberger et al., 2012) and humans (Albers et al., 2015).

5. Conclusions

In summary, our data are consistent with the view that the AD-related impairment of visual processing is caused by a complex change in the excitation/inhibition balance in the primary visual cortex. The

latter comprises both a store dysfunction-mediated increase in neurotransmitter release from the glutamatergic axons, causing an overall increase in visual responsiveness, and an amyloid/neuroinflammation-mediated dysfunction of inhibitory interneurons, underlying the impairment of visual tuning and of the stimulus-induced suppression of spontaneous activity.

Supplementary data to this article can be found online at https://doi.org/10.1016/j.nbd.2018.10.015.

Competing interests

The authors declare that they have no competing interests.

Funding

This work was supported by VolkswagenStiftung Grant 90233 (to O.G.) as well as fortüne Grant 2200 (to B.B.).

Authors' contributions

O.G. conceived the study. N.A., B.B. and O.G. designed and/or performed experiments, P.M. contributed to data analyses. N.A. and O.G. wrote the manuscript. All authors analyzed data and commented on the manuscript.

Acknowledgements

We thank E. Zirdum, A.Weible and K. Schoentag for technical assistance. The PS45 mice were originally obtained from M. Staufenbiel.

References

Albers, M.W., et al., 2015. At the interface of sensory and motor dysfunctions and Alzheimer's disease. Alzheimers Dement. 11, 70–98.
Atallah, B.V., et al., 2012. Parvalbumin-expressing interneurons linearly transform cortical responses to visual stimuli. Neuron 73, 159–170.
Bakker, A., et al., 2012. Reduction of hippocampal hyperactivity improves cognition in amnestic mild cognitive impairment. Neuron 74, 467–474.
Bezprozvanny, I., Mattson, M.P., 2008. Neuronal calcium mishandling and the pathogenesis of Alzheimer's disease. Trends Neurosci. 31, 454–463.
Busche, M.A., et al., 2008. Clusters of hyperactive neurons near amyloid plaques in a mouse model of Alzheimer's disease. Science 321, 1686–1689.
Chakroborty, S., Stutzmann, G.E., 2014. Calcium channelopathies and Alzheimer's disease: insight into therapeutic success and failures. Eur. J. Pharmacol. 739, 83–95.
Chen, T.W., et al., 2013. Ultrasensitive fluorescent proteins for imaging neuronal activity. Nature 499, 295–300.
Cronin-Golomb, A., et al., 1991. Visual dysfunction in Alzheimer's disease: relation to normal aging. Ann. Neurol. 29, 41–52.
Daulatzai, M.A., 2015. Olfactory dysfunction: its early temporal relationship and neural correlates in the pathogenesis of Alzheimer's disease. J. Neural Transm. (Vienna) 122, 1475–1497.
Deneux, T., Grinvald, A., 2017. Milliseconds of sensory input abruptly modulate the dynamics of cortical states for seconds. Cereb. Cortex 27, 4549–4563.
Garaschuk, O., et al., 2006. Targeted bulk-loading of fluorescent indicators for two-photon brain imaging in vivo. Nat. Protoc. 1, 380–386.
Gates, G.A., et al., 2008. Central auditory dysfunction in older persons with memory impairment or Alzheimer dementia. Arch. Otolaryngol. Head Neck Surg. 134, 771–777.
Goussakov, I., et al., 2010. NMDA-mediated Ca^{2+} influx drives aberrant ryanodine receptor activation in dendrites of young Alzheimer's disease mice. J. Neurosci. 30, 12128–12137.
Grienberger, C., et al., 2012. Staged decline of neuronal function in vivo in an animal model of Alzheimer's disease. Nat. Commun. 3, 774.
Haberman, R.P., et al., 2017. Targeting Neural Hyperactivity as a Treatment to Stem Progression of Late-Onset Alzheimer's Disease. Neurotherapeutics 14, 662–676.
Hardy, J., 1997. Amyloid, the presenilins and Alzheimer's disease. Trends Neurosci. 20, 154–159.
Hermes, M., et al., 2010. Intracellular calcium signalling in Alzheimer's disease. J. Cell. Mol. Med. 14, 30–41.
Kuchibhotla, K.V., et al., 2014. Neurofibrillary tangle-bearing neurons are functionally integrated in cortical circuits in vivo. Proc. Natl. Acad. Sci. U. S. A. 111, 510–514.
Lee, S.H., et al., 2012. Activation of specific interneurons improves V1 feature selectivity and visual perception. Nature 488, 379–383.
Lerdkrai, C., Garaschuk, O., 2018. Role of presynaptic calcium stores for neural network dysfunction in Alzheimer's disease. Neural Regen. Res. 13, 977–978.
Lerdkrai, C., et al., 2018. Intracellular Ca^{2+} stores control in vivo neuronal hyperactivity in a mouse model of Alzheimer's disease. Proc. Natl. Acad. Sci. U. S. A. 115, E1279–E1288.
Liebscher, S., et al., 2016. Selective Persistence of Sensorimotor Mismatch Signals in Visual Cortex of Behaving Alzheimer's Disease mice. Curr. Biol. 26, 956–964.
Martins Da Silva, A., Leal, B., 2017. Photosensitivity and epilepsy: current concepts and perspectives-a narrative review. Seizure 50, 209–218.
Mattson, M.P., 2010. ER calcium and Alzheimer's disease: in a state of flux. Sci. Signal. 3, pe10.
Mesholam, R.I., et al., 1998. Olfaction in neurodegenerative disease: a meta-analysis of olfactory functioning in Alzheimer's and Parkinson's diseases. Arch. Neurol. 55, 84–90.
Minkeviciene, R., et al., 2009. Amyloid beta-induced neuronal hyperexcitability triggers progressive epilepsy. J. Neurosci. 29, 3453–3462.
Niell, C.M., Stryker, M.P., 2008. Highly selective receptive fields in mouse visual cortex. J. Neurosci. 28, 7520–7536.
Niell, C.M., Stryker, M.P., 2010. Modulation of visual responses by behavioral state in mouse visual cortex. Neuron 65, 472–479.
Palop, J.J., Mucke, L., 2016. Network abnormalities and interneuron dysfunction in Alzheimer disease. Nat. Rev. Neurosci. 17, 777–792.
Palop, J.J., et al., 2006. A network dysfunction perspective on neurodegenerative diseases. Nature 443, 768–773.
Palop, J.J., et al., 2007. Aberrant excitatory neuronal activity and compensatory remodeling of inhibitory hippocampal circuits in mouse models of Alzheimer's disease. Neuron 55, 697–711.
Petersen, C.C., et al., 2003. Interaction of sensory responses with spontaneous depolarization in layer 2/3 barrel cortex. Proc. Natl. Acad. Sci. U. S. A. 100, 13638–13643.
Risacher, S.L., et al., 2013. Visual contrast sensitivity in Alzheimer's disease, mild cognitive impairment, and older adults with cognitive complaints. Neurobiol. Aging 34, 1133–1144.
Rizzo, M., et al., 2000. Vision and cognition in Alzheimer's disease. Neuropsychologia 38, 1157–1169.
Schmid, L.C., et al., 2016. Dysfunction of somatostatin-positive interneurons associated with memory deficits in an Alzheimer's disease model. Neuron 92, 114–125.
Shen, J., Kelleher III, R.J., 2007. The presenilin hypothesis of Alzheimer's disease: evidence for a loss-of-function pathogenic mechanism. Proc. Natl. Acad. Sci. U. S. A. 104, 403–409.
Siskova, Z., et al., 2014. Dendritic structural degeneration is functionally linked to cellular hyperexcitability in a mouse model of Alzheimer's disease. Neuron 84, 1023–1033.
Steiner, H., Haass, C., 2000. Intramembrane proteolysis by presenilins. Nat. Rev. Mol. Cell Biol. 1, 217–224.
Stosiek, C., et al., 2003. In vivo two-photon calcium imaging of neuronal networks. Proc. Natl. Acad. Sci. U. S. A. 100, 7319–7324.
Stothart, G., et al., 2015. Early visual evoked potentials and mismatch negativity in Alzheimer's disease and mild cognitive impairment. J. Alzheimers Dis. 44, 397–408.
Tada, M., et al., 2014. A highly sensitive fluorescent indicator dye for calcium imaging of neural activity in vitro and in vivo. Eur. J. Neurosci. 39, 1720–1728.
Tandon, A., Fraser, P., 2002. The presenilins. Genome Biol. 3 (reviews3014).
Verret, L., et al., 2012. Inhibitory interneuron deficit links altered network activity and cognitive dysfunction in Alzheimer model. Cell 149, 708–721.
Zeger, S.L., Liang, K.Y., 1986. Longitudinal data analysis for discrete and continuous outcomes. Biometrics 42, 121–130.
Zhang, C., et al., 2009. Presenilins are essential for regulating neurotransmitter release. Nature 460, 632–636.